Effect of Crystalline Microstructure Near the Particle/Matrix Interface on the Toughening of Syndiotactic Polystyrene/Polyamide-6 Blends

Byung Il Kang, Sobha V. Nair, Hoichang Yang, Ho Sun Lim, Dae Ho Lee, Kilwon Cho

Department of Chemical Engineering, Polymer Research Institute, Pohang University of Science and Technology, Pohang 790-784, Korea

Received 22 June 2007; accepted 2 December 2007
DOI 10.1002/app.27870
Published online 21 February 2008 in Wiley InterScience (www.interscience.wiley.com).

ABSTRACT: Toughening behavior of semicrystalline polymers was investigated using syndiotactic polystyrene (sPS)/polyamide 6(PA-6) blends compatibilized with maleic-anhydride functionalized poly (styrene-*b*-(ethylene-*co*-butylene)-*b*-styrene) SEBS-MA triblock copolymer. The effect of interparticle distance and crystal microstructure near the particle/matrix interface of the blends were studied. The morphology studies revealed that the size and interparticle distance of the dispersed PA-6 particles decreased with increasing SEBS-MA concentration. sPS/PA-6 blends exhibited sharp brittle-ductile transitions at a critical interparticle distance of 0.25 μm. With the increase of the compatibilizer concentration beyond a certain level, it was observed that the further addition resulted in decreased impact strength. This could be attributed to the formation of a separate phase in the matrix by the additional SEBS added. The TEM studies showed that when the interparticle distance is below 0.25 μm, the matrix ligaments between the inclusions will be filled with well-oriented crystalline material of reduced plastic resistance. From DSC and X-ray diffraction studies of model thin films, it was found that the fraction of small and imperfect crystallites near the particle/matrix interface increased with decreasing interparticle distance. This resulted in decreased yield stress of the whole matrix with increasing concentration of SEBS-MA accompanied by changes in the fracture mode from brittle to tough. © 2008 Wiley Periodicals, Inc. J Appl Polym Sci 108: 2734–2747, 2008

Key words: syndiotactic polystyrene; polyamide 6; toughening; crystalline microstructure; interface

INTRODUCTION

Syndiotactic polystyrene (sPS), which is a relatively new semi-crystalline polymer has attracted significant interest because of its unique physical properties like high heat resistance, excellent chemical resistance, high degree of crystallinity, low specific gravity, and good dielectric properties.[1–6] However, the polymer has certain major drawbacks such as high brittleness, i.e., poor impact strength.[7] Improvement of these properties of sPS would certainly widen the spectrum of applications. Our survey of literature revealed that a few studies have been conducted to improve the impact strength of sPS.[8–12]

The toughening of semicrystalline polymers with rubber particles has been an area of active research over the past few years.[13–24] Most of these studies reported the effect of parameters such as rubber particle size, volume fraction, and interparticle distance (ID) on toughening. On the basis of his pioneering investigations on the toughening of polyamides, Wu[14,15] became the first to introduce the criterion of ID in the toughening of semi-crystalline polymers. According to his experimental observations, he proposed that the matrix ligament thickness between the particles is the key parameter for the toughening of semicrystalline polymers. He also found that a sharp brittle-tough transition occurs when the average ID (matrix ligament thickness) is below a certain critical value (ID_c). This critical value is independent of rubber volume fraction and particle size, and is the property of matrix alone. Borggreve et al.[25] explained the critical particle distance with a transition from plane strain to plane stress conditions. Plane stress conditions leads to shear yielding, resulting in tough blends. When the ID is larger than the critical value, the plane strain to plane stress transition will not take place and as a result the matrix ligaments fail in a brittle manner.

Recently Muratoglu et al.[16,17] proposed a new morphological explanation for Wu's observations. They suggested that the toughness jumps occurring in rubber-modified polyamides is related to the changes in matrix morphology induced by the rubber matrix-interface as the ID is varied. It was

Correspondence to: K. Cho (kwcho@postech.ac.kr).
Contract grant sponsors: Center for Nanostructured Materials Technology of the Ministry of Science and Technology of Korea; contract grant number: 07K1501-01010.

Journal of Applied Polymer Science, Vol. 108, 2734–2747 (2008)

observed by TEM that in nylon 66 modified with ethylene-propylene rubber, when ID $<$ ID$_c$ (0.3 μm), the nylon matrix within the ligaments has a specific crystallographic orientation with the crystalline lamellae being arranged perpendicular to the interfaces of adjacent rubber particles within the matrix. Such oriented layers of lamellae extended $\sim$ 0.15 μm away from each nylon/rubber interface, and in films of ligament thickness less than 0.3 μm, results in preferred orientation of the lamellae throughout the film. When the ligament thickness exceeded 0.3 μm, crystallites of random orientation were found to populate the interior to afford a matrix with high deformation resistance leading to a brittle failure. However, a drastic increase in the toughness of semicrystalline polymer blends cannot be explained only by the preferentially oriented lamellae around the particles. The crystallization behavior of the matrix polymer is affected substantially by the increase of nucleation sites resulting from the addition of modifying particles and the confined morphology between well dispersed particles. Thus, when semi crystalline polymers are crystallized from melt, population of different crystals can exist. Specifically, for sPS crystallized from the melt, DSC curves show three separate melting endotherms, suggesting that there exist different types of crystals in the matrix.[26] Therefore, while considering the toughening behavior of semicrystalline polymers, besides the preferentially oriented lamellae, the crystal imperfection around the particles should also be taken into account. In our study, the effect of crystal imperfection near the particles on the toughening behavior of sPS has been verified.

The major disadvantage of rubber modification for improved toughness is that it reduces the modulus and tensile strength that in turn affects the end use applications of the polymer. Another approach towards attaining toughened polymers is the incorporation of rigid thermoplastic particles instead of rubber, which results in improved impact strength with little or no reduction in the stiffness. This procedure, termed as the rigid–rigid polymer-toughening concept has been used to toughen various thermoplastic polymers.[27–33]

The present study deals with the toughening of sPS by the incorporation of a thermoplastic polymer. Since the melt processing temperature of sPS is very high (over 280°C), thermoplastic polymers to be incorporated for toughening should be thermally stable at high temperatures. For this reason, we chose PA-6 as the thermoplastic component. Because of the differences in their polarity and solubility parameters, these two polymers are immiscible. The morphology of the dispersed particles as well as the interfacial adhesion between the dispersed phase and the matrix plays a major role in determining the mechanical properties of the blend. This can be achieved by the addition of compatibilizers to mediate attractive interactions between the immiscible components of the blend.[34–37] The compatibilizer employed in the present study is a copolymer of atactic polystyrene (a-PS)-*b*-poly(ethylene-*co*-butylene)-*b*-atactic polystyrene (SEBS) modified by reaction with maleic anhydride (referred to SEBS-MA), which has excellent thermal stability at high temperatures. During melt mixing conditions, SEBS-MA becomes grafted with PA-6 by reaction involving the maleic anhydride groups on SEBS-MA with the amine end groups on PA-6.[36,38] It has been recently reported that sPS is miscible with aPS.[26,39] Hence, SEBS-MA is expected to be a potential compatibilizer for sPS/PA-6 blends.

We report the results from thermal, morphological, crystalline and mechanical properties of sPS/PA-6 blends with respect to the concentration of SEBS-MA (the compatibilizer) used. Our study focuses on the effects of ID and crystalline microstructure near the particle/matrix interface on the brittle-tough transition of sPS/PA-6 blends compatibilized with SEBS-MA.

EXPERIMENTAL

Materials

The sPS was obtained from Dow Chemical, USA and Polyamide-6 (PA-6) was obtained from BASF as UltramidB3. Kraton FG 1901X here referred as SEBS-MA, which was used as compatibilizer was obtained from Shell Chemicals. The functionalized SEBS contains $\sim$ 2% by weight maleic anhydride groups attached to EB mid blocks. The aminosilane compound (Aldrich) used in the model study was γ-aminopropylethoxysilane.

Blend preparation

All the polymer samples were completely dried in a vacuum oven at 80°C for 20 h before blending. The samples were melt blended at 290°C for 15 min and injection molded into dumbbells in a Mini-Max molder (CS-NMX, Custom Scientific Instruments). The weight ratios of sPS/PA-6 blends were 90/10, 80/20, and 70/30 and the compatibilizer concentrations studied were 0, 2, 5, 7, and 10 wt % for each sPS/PA-6 weight ratio.

Electron microscopy

The morphology of the blends were analyzed using scanning electron microscopy (SEM) [FE-SEM Hitachi 4200] and transmission electron microscopy (TEM; JEOL 1200EX). Specimens for particle size analysis

using SEM were cryo-fractured and were coated with a thin layer of gold-palladium. For TEM, thin section of bulk region was obtained using a cryogenic ultramicrotome system (RMC, MT-7000). Then the sectioned films were picked up on 300-mesh copper grids and stained using the vapor of either 2 wt % aqueous osmium tetroxide (OsO_4) or ruthenium tetroxide (RuO_4) solution to increase phase contrast.

Mechanical testing

Test specimens for the tensile measurements were prepared from 1-mm thick plates according to ASTM D 638. The Young's modulus was measured by universal tensile test machine (Instron 4206) at room temperature with six specimens for each sample. The strain rate was 5.08 cm min^{-1}. The Charpy impact strength (ASTM D256) was determined using a single-edge notched specimen (notch radius 0.25 mm) at room temperature.

Thermal analysis

Thermal analysis was done using Perkin–Elmer DSC-7 under nitrogen atmosphere. Samples were heated to 300°C and kept for 5 min to eliminate the influence of thermal history. They were then cooled to −70°C and reheated to 290°C at a rate of 20°C min^{-1}. Melting temperature (T_m) was determined from the second heating curve and crystallization temperature (T_c) from the cooling curve. The normalized crystallinity of sPS was determined from the following equation

$$\chi_c = \frac{\Delta H_f / \Delta H_f^0}{w} \times 100\%$$

where, ΔH_f is the melting enthalpy of the blend, ΔH_f^0 is the melting enthalpy of 100% crystalline sPS (ΔH_f^0 = 53 J g^{-1}),[40] and w is the weight fraction of sPS in the blend.

Thin film study

To investigate the effect of tethered PS chains around particles on the crystalline microstructure of sPS in blend, thin films were prepared on silicon wafers and grazing incidence X-ray diffraction (GIXD) was performed on these thin sPS film as a model system of this study. The change of crystalline microstructure in the prepared films was qualitatively determined in the reflection mode, while the films were still lying flat on the silicon substrate. To investigate the difference of crystalline microstructure near the interface of sPS and silicon wafer with and without SEBS-MA tethered chain, SEBS-MA thin film assemblies with a typical thickness of 50 nm have been prepared. Thin films were prepared by spin coating the solutions onto silicon wafers with a rotation speed of 2500 rpm in all the cases. Silicon wafers were grafted with γ-aminopropyltriethoxysilane (γ-APS) so that their surfaces contain amino groups, which can react with the SEBS-MA chains. We limited the grafting time to 18 h because no significant changes were observed beyond the fist 18 h of grafting time. The unbounded polymer was removed by multiple washing with toluene, including washing in an ultrasonic bath.

Solution of sPS (1 wt %) was prepared in hot xylene under argon to avoid the oxidation of polymer. sPS films (∼ 100 nm) were deposited by spin coating on to hot glass plates from solution to prevent polymer precipitation. After drying for 12 h to remove any excess solvent, the sPS film was heated above the melting temperature to remove solvent induced sPS crystal form. Then the sPS film was floated off the glass plate onto the surface of a water bath and picked up on the SEBS-MA coated γ-APS grafted wafers.

The sPS/SEBS-MA/γ-APS grafted wafer assembly was then annealed under vacuum to avoid the oxidation of sPS. After melting sPS films at 290°C for 10 min, the sample stage was moved rapidly to a second heating stage kept at 180°C and was subjected to an isothermal crystallization for 1 h. Figure 1 is the schematic representation showing the steps for the preparation of model thin film, sPS/tethered SEBS blend film on silicon wafer. The diffraction patterns for the interface layer of sPS films were obtained by GIXD. This experiment was conducted using synchrotron X-ray radiation source (3C2 beam line, wave length 1.598 Å) at the Pohang accelerator laboratory, Pohang, Korea.

RESULTS AND DISCUSSION

Morphology of simple and compatibilized blends

Figure 2 shows the SEM micrographs of simple sPS/PA-6 80/20 blends and those compatibilized with varying concentration of SEBS-MA. The samples are cryogenically fractured and PA-6 phase has been preferentially etched using formic acid at 40°C. The simple blends exhibit a two-phase morphology with PA-6 dispersed in the continuous sPS phase. The cavities from which PA-6 has been etched are perfectly clear and smooth indicating the absence of adhesion between the dispersed phase and the matrix. This suggests that sPS/PA-6 blends are incompatible. With the addition of SEBS-MA, the dimensions of the dispersed PA-6 phase have been decreased obviously. The average particle diameter for sPS/PA-6 blends with respect to SEBS-MA concentration

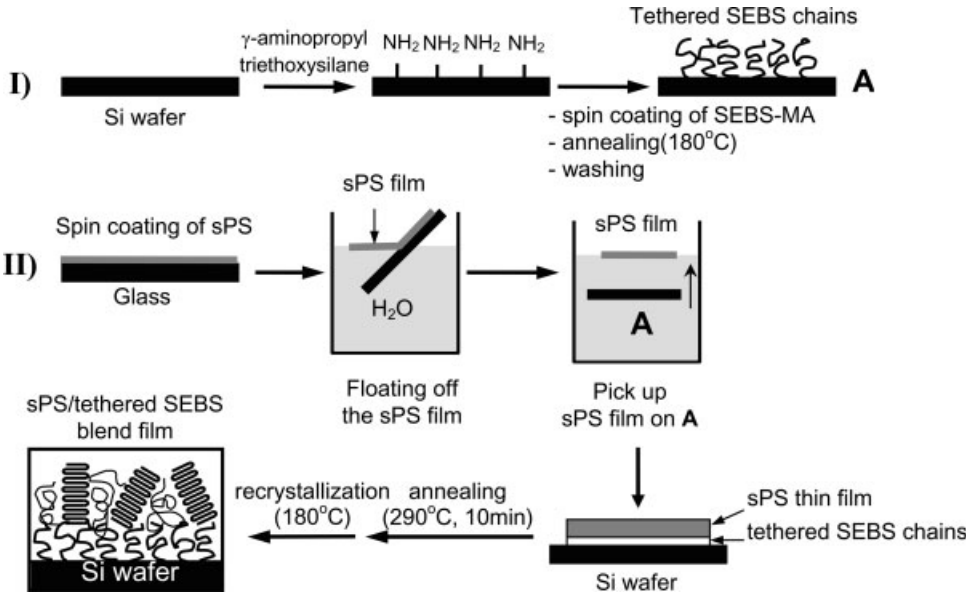

Figure 1 Schematic representation showing the steps of preparation of model thin film (sPS/tethered SEBS blend film on Si wafer) for X-ray diffraction studies. (I) Tethering SEBS chains on amine-modified Si wafer (A). (II) Floating off sPS film and picking up of sPS film on A followed by annealing at 290°C for 10 min and recrystallization at 180°C.

is shown in Figure 3. The addition of the compatibilizer beyond 2 wt % has resulted in a substantial reduction of the domain size and a uniform distribution of the dispersed phase. It can be observed from Figure 3 that in the case of sPS/PA-6 80/20 and 70/30 blends, addition of 5 wt % SEBS-MA causes a sig-

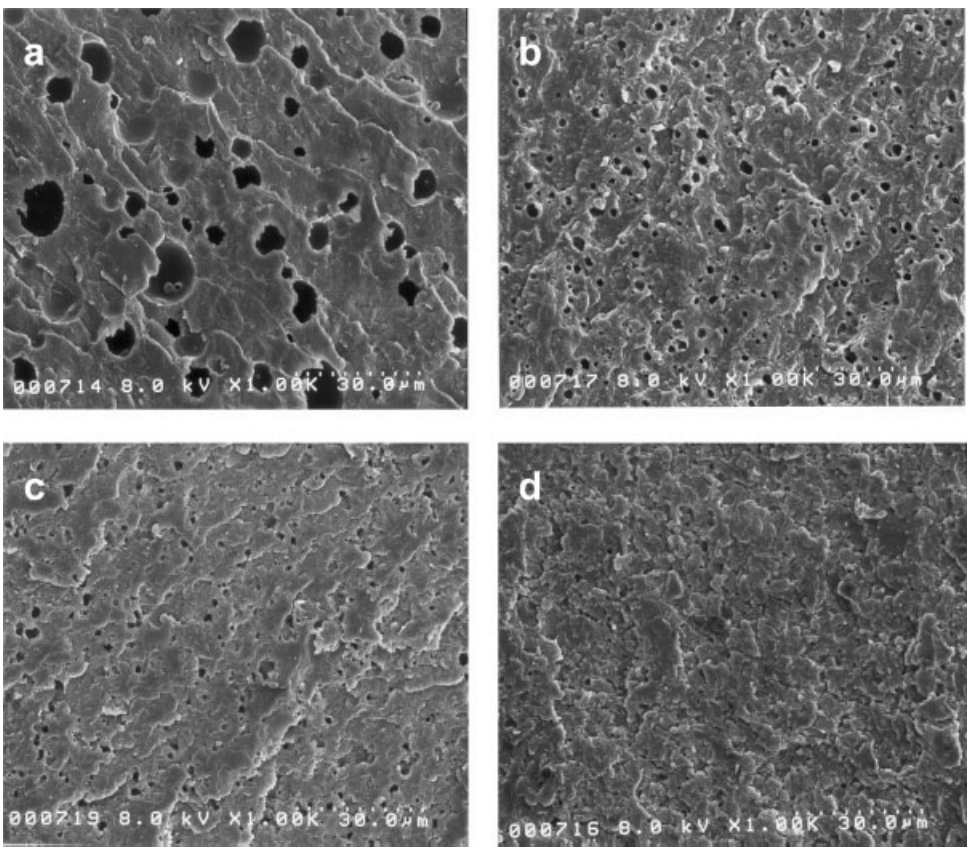

Figure 2 SEM micrographs of simple and SEBS-MA compatibilized sPS/PA-6 (80/20) blends. SEBS-MA content (a) 0 wt % (b) 2 wt % (c) 5 wt %, and (d) 7 wt %.

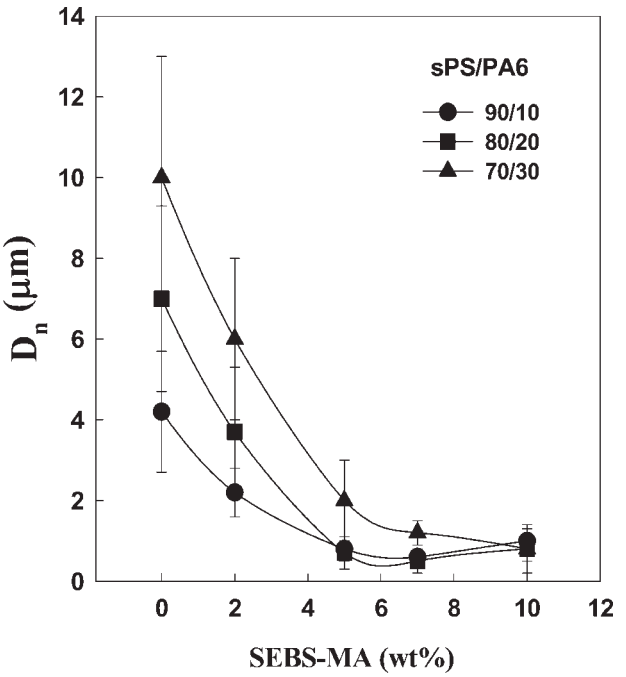

Figure 3 Number average domain diameter (Dn) of the sPS/PA-6 blends as a function of sPS/PA-6 weight ratio and SEBS-MA content.

nificant reduction in the domain size. Further addition of the compatibilizer does not contribute towards particle size reduction that almost levels off above 5 wt % addition. In contrast to these blend compositions, sPS/PA-6 90/10 shows a continuous decrease in Dn up to the addition of 7 wt % SEBS-MA and then levels off.

Additional insight into the blend morphology and the interfacial activity of SEBS-MA is obtained from TEM. The TEM micrographs of sPS/PA-6 80/20 blends compatibilized with 5, 7, and 10 wt % of SEBS-MA are shown in Figure 4(a–c). When SEBS-MA is added to the system, it can be positioned in three ways: SEBS-MA domains dispersed in the PA-6 phase, SEBS-MA dispersed in the sPS phase and SEBS-MA located at the interface between sPS and PA-6 phases. The careful inspection of Figure 4(a) reveals a thin dark layer of SEBS-MA surrounding the PA-6 particles. This indicates that the compatibilizer prefers to reside at the interface between sPS and PA-6. The addition of 7 wt % of SEBS-MA forms a thick sheath of compatibilizer surrounding the PA-6 particles as observed in Figure 4(b). It is also observed that the thick SEBS-MA sheathed PA-6 particles tend to promote aggregates. It is to be noted that in the case of addition of 5 and 7 wt % compatibilizer, no individual SEBS-MA phase is observed. However, on further addition of SEBS-MA (10 wt %), small black particles can be seen in the sPS matrix [Fig. 4(c)], which are most probably the residual dispersed SEBS-MA. Therefore when the SEBS-MA concentration exceeds 7 wt %, the additional compatibilizer forms a separate phase in the sPS matrix.

Tensile properties

Typical stress–strain curves obtained at room temperature for the neat and toughened sPS are shown in Figure 5. Up to 2 wt % SEBS-MA, the blends exhibit a linear stress–strain behavior ending in a brittle failure. With the addition of 5 and 7 wt % SEBS-MA, a pronounced nonlinear stress–strain curve is obtained, which indicates the signs of plastic deformation. In these cases, the crack after initiation propagates in a stable crack growth. This confirms that the compatibilized blends exhibit much higher fracture toughness than neat sPS and sPS/PA-6 blends. The flat portion of the stress–strain curves in the high concentration SEBS-MA specimens suggests that, before crack growth a large-scale plastic deformation takes place in these blends. The overall stress of the blends as a function of SEBS-MA content is depicted in Figure 6, which shows that overall stress of the binary sPS/PA-6 blends, is slightly decreased by the addition of PA-6. As the concentration of SEBS-MA increases, the overall stress shows a gradual decrease. Till 2 wt %, this reduction is not substantial, but is followed by a dramatic reduction between 2 and 5 wt %, which is associated with a change in fracture mode from brittle to tough as discussed later. Therefore, the overall stress indicates the breaking stress when the SEBS-MA content is less than 2 wt % and the yield stress when the SEBS-MA content is greater than 5 wt %.

The Young's modulus of the blends with varying SEBS-MA concentration is plotted in Figure 7. Pure sPS has a Young's modulus of 3.2 Gpa and that of pure PA-6 is 2.8 Gpa. The Young's modulus of the binary blends sPS/PA-6 shows an intermediate value between the two components. With the addition of SEBS-MA the Young's modulus of the system decreases gradually. It can be seen from Figure 7 that up to 7 wt % addition of the compatibilizer the extent of reduction in the modulus is low, with a drastic reduction occurring at 10 wt % SEBS-MA. It has already been observed from the TEM micrographs (Fig. 4) that beyond 7 wt %, the addition of SEBS-MA results in the formation of a separate phase. Hence, the significant reduction in the Young's modulus with 10 wt % SEBS-MA addition is preferentially due to the existence of individual SEBS-MA domains in the sPS matrix.

Impact properties

Izod impact strength

The notched impact strength of the blends at room temperature is plotted as a function of sPS/PA-6

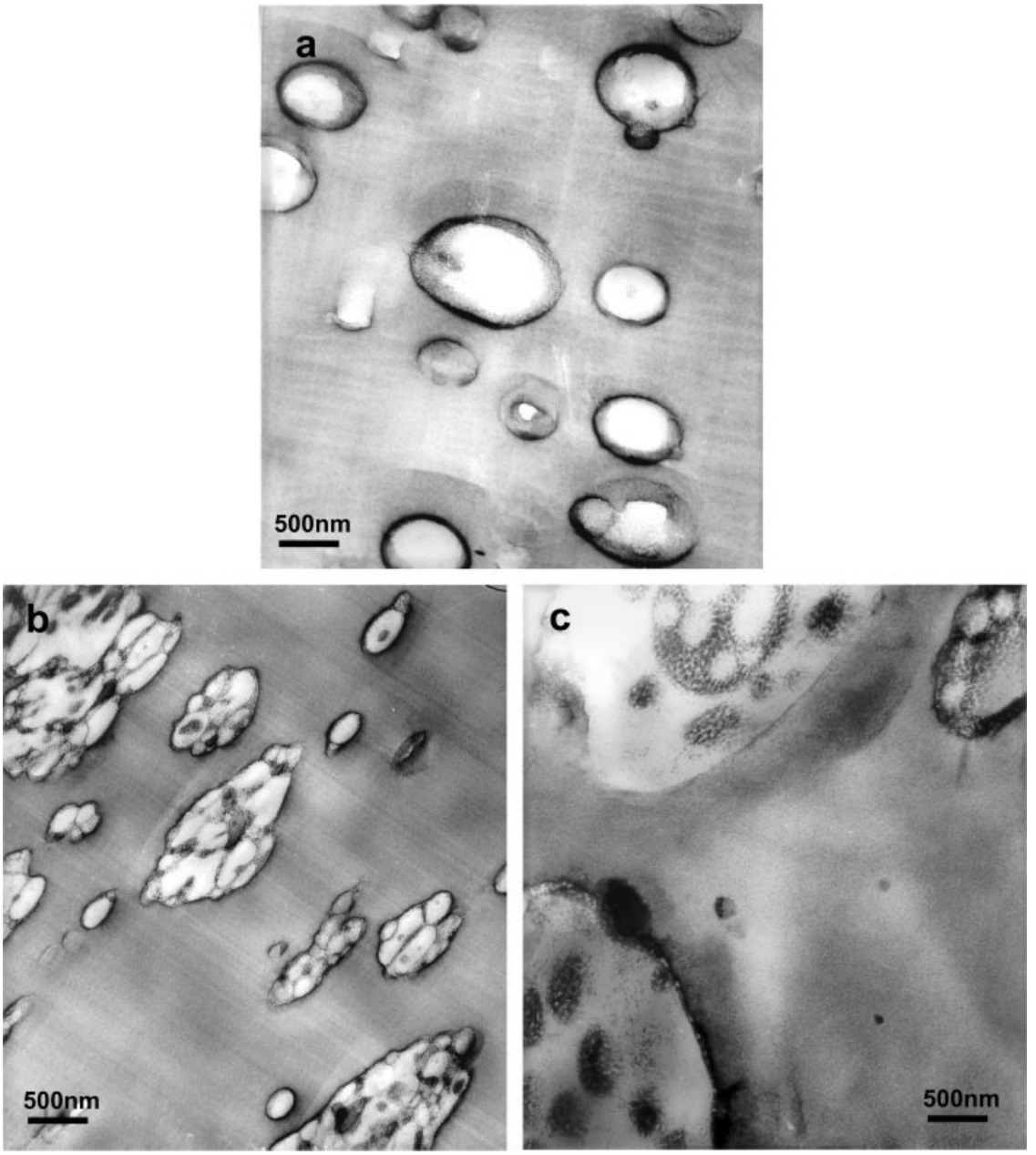

Figure 4 TEM micrographs of sPS/PA-6 blends. SEBS-MA content (a) 5 wt % (b) 7 wt %, and (c) 10 wt %.

composition and SEBS-MA content in Figure 8. Simple blends exhibit slightly better impact properties when compared with pure sPS. The impact strength increases with compatibilizer concentration in all the blends irrespective of their compositions. Up to 2 wt %, the addition of compatibilizer has resulted only in a slight improvement of impact strength. With the addition of 5 wt % SEBS-MA, there is a drastic increase in the impact strength in all the blends. It is evident from the figure that in all the compositions studied, the impact strength increases regularly with PA-6 content up to 2 wt % SEBS-MA addition. However, when the compatibilizer loading exceeds 2 wt %, the improvement in the impact strength varies with PA-6 content. In the case of sPS/PA-6 80/20 and 70/30 blends, there is a strong jump of impact strength occurring between 2 and 5 wt % SEBS-MA. For sPS/PA-6 90/10 blends, the abrupt improvement in impact strength occurs at 7 wt % compatibilizer loading. All the blends exhibit the maximum impact strength at a compatibilizer concentration of 7 wt %. At 10 wt % compatibilizer loading, there is a substantial decrease of impact strength. The improvement in impact strength upon

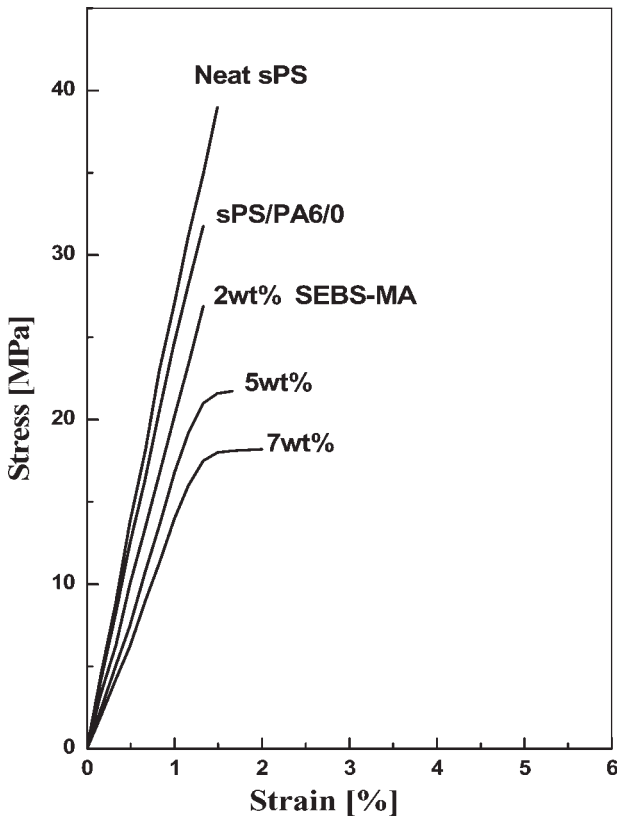

Figure 5 Stress-strain curves of neat sPS and sPS/PA-6 (80/20) blends compatibilized with SEBS-MA.

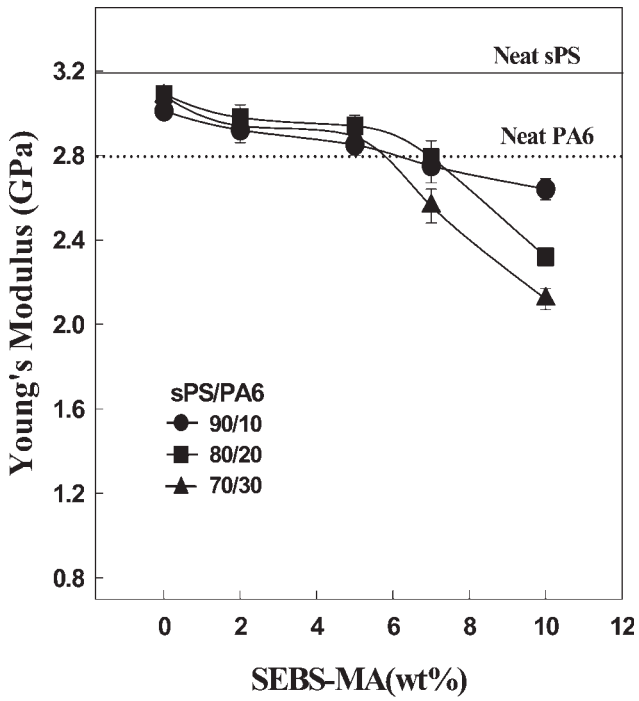

Figure 7 Young's modulus of sPS/PA-6 blends as a function of SEBS-MA content.

compatibilization is due to the change in fracture mode from brittle to tough, which is discussed in the criterion of toughening to sPS/PA-6 blends.

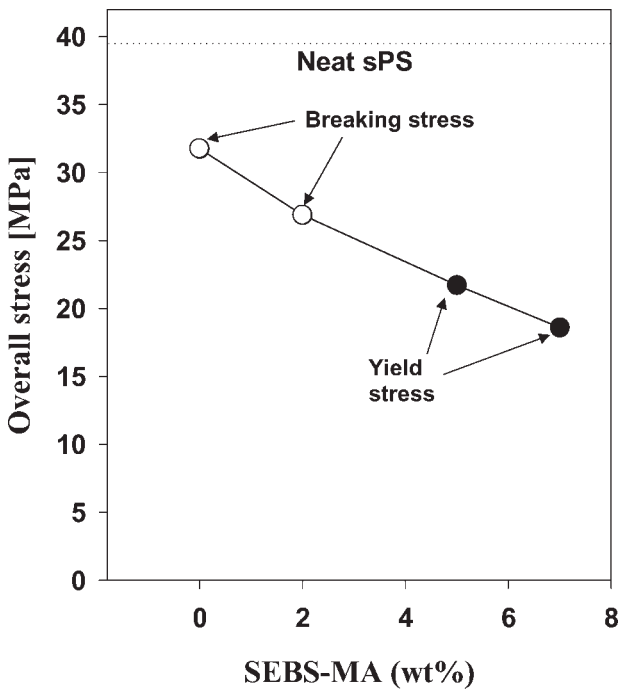

Figure 6 Overall stress of sPS/PA-6 (80/20) blends as a function of SEBS-MA content.

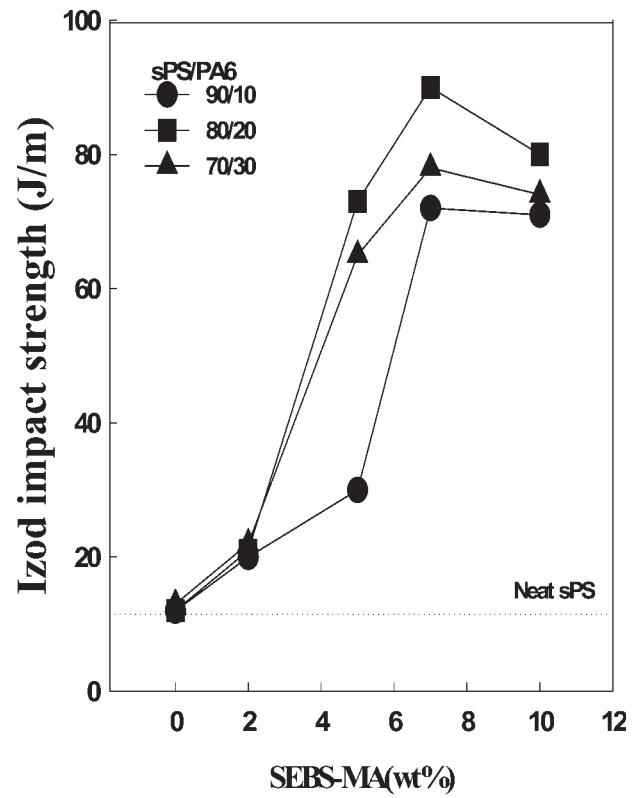

Figure 8 Notched impact strength of the sPS/PA-6 blends as a function of SEBS-MA content.

Hence in the case of sPS/PA-6 90/10 blends, the change in fracture mode occurs between 5 and 7 wt % compatibilizer concentration, whereas in the case of sPS/PA-6 80/20 and 70/30 blends, the toughness jump is observed between 2 and 5 wt % SEBS-MA concentration.

Relevance of blend morphology in the toughening of sPS/PA-6 blends

In addition to the change in fracture mode, the improvement in toughness at higher compatibilizer loading can also be attributed to the reduction of PA-6 particle size (Figs. 2 and 3), their uniform dispersion and the better interfacial adhesion between the dispersed phase and the matrix. The maximum toughness exhibited by the blends at 7 wt % SEBS-MA can be explained on the basis of morphology obtained from TEM analysis [Fig. 4(b)]. TEM micrographs revealed that the SEBS-MA is not only located at the interface between the sPS and PA-6, where it lowers the interfacial tension thereby improving the adhesion between both the phases, but forms together with the PA-6 dispersed particles, a complex structure. It is clearly evident from the Figure that the EB blocks of SEBS-MA besides forming spherical or layered domains, penetrate obviously into the pure PA-6 particles joining them into complex aggregates with a ''honeycomb-like'' morphology. Thus it can act as an impact modifier as it is well known that thermoplastic elastomers are very effective toughening agents. When the compatibilizer concentration is 10 wt %, small particles are observed in the sPS matrix, which could be the residual dispersed SEBS-MA forming a separate phase. Recently Li et al.[9] reported a decrease of impact strength in sPS/PA-6 blends compatibilized with sulfonated syndiotactic polystyrene(SsPS-H) beyond 5 wt % addition of the compatibilizer. According to their results, the excess SsPS-H could remain in an agglomerated form in the blend due to strong interactions between the sulfonate groups, providing a stress concentration points in the testing, which ultimately leads to a decreased toughness. Li and Li[41] obtained a similar result for polyamide-1010/a-PS blends compatibilized by sulfonated atactic polystyrene (SaPS-H) and has attributed the phenomenon to the existence of the ''loose interface'' between the two phases formed by the introduction of the excess SPS-H. Therefore, in our case the residual dispersed SEBS-MA forming a separate phase may reduce the effectiveness of toughening and could lead to decreased impact strength at higher compatibilizer concentration. Thus, the morphology of the blends plays a major role in the toughening mechanism.

Fracture surface morphology of the impact specimens

Figure 9 shows the variation in morphology at the impact-fractured surfaces of the sPS/PA-6 blends compatilbilized with SEBS-MA copolymer. The morphology of sPS/PA-6 80/20 blends compatibilized with 2 wt % SEBS-MA shown in Figure 9(a,b) indicates that the dispersed particles are strongly embedded in the matrix. The surfaces after fracture are not smooth indicating good adhesion. In Figure 9(b) (the higher magnification of 9a) an interfacial layer can be observed around each particle without any voids between the particles and the matrix, which provides a direct evidence of the interfacial activity of SEBS-MA leading to an improved interfacial adhesion. The morphology of sPS/PA-6 80/20 blends compatibilized with 5 wt % SEBS-MA is shown in Figure 9(c,d) where we can observe a yielding like matrix deformation and ductile tearing. This suggests that, the massive deformation progress in the whole matrix. It is clearly evident from Figure 9(d) [higher magnification of Fig. 9(c)] that the PA-6 particles at the fracture surface is covered with a layer of compatibilizer spreading from the particle surface into the matrix phase with fibrils holding the particles in the matrix, which confirms the yielding deformation of the matrix at 5 wt % compatibilizer loading. Thus the improved interfacial adhesion enables the applied stress to be transferred through the dispersed phase as well. It can also be suggested that the relatively fine dispersions of PA-6 surrounded by the SEBS-MA interface also provide effective stress interactions in enhancing shear deformation by relieving the hydrostatic stress via cavitation.[42,43]

Crystalline microstructure

DSC study

It is widely accepted that the crystalline microstructure of semicrystalline polymers plays a significant role in determining their mechanical properties and fracture behavior. The effect of addition of second phase particles on the crystallization behavior and spherulite morphology of semi crystalline polymers and their blends has been reported.[12,44–46] In the case of sPS blends, aPS portion of the compatibilizer (SEBS-MA) employed is miscible with the sPS and results in varying morphology and interfacial properties with loading concentration. This along with the change of ID affects the crystalline microstructure of the sPS matrix. To evaluate the extent to which PA-6 and SEBS-MA influence the crystalline microstructure of sPS blends, DSC analyses were performed. The DSC thermograms of sPS/PA-6 blends with varying compatibilizer loading is shown in Figure 10 which clearly demonstrates that, all the

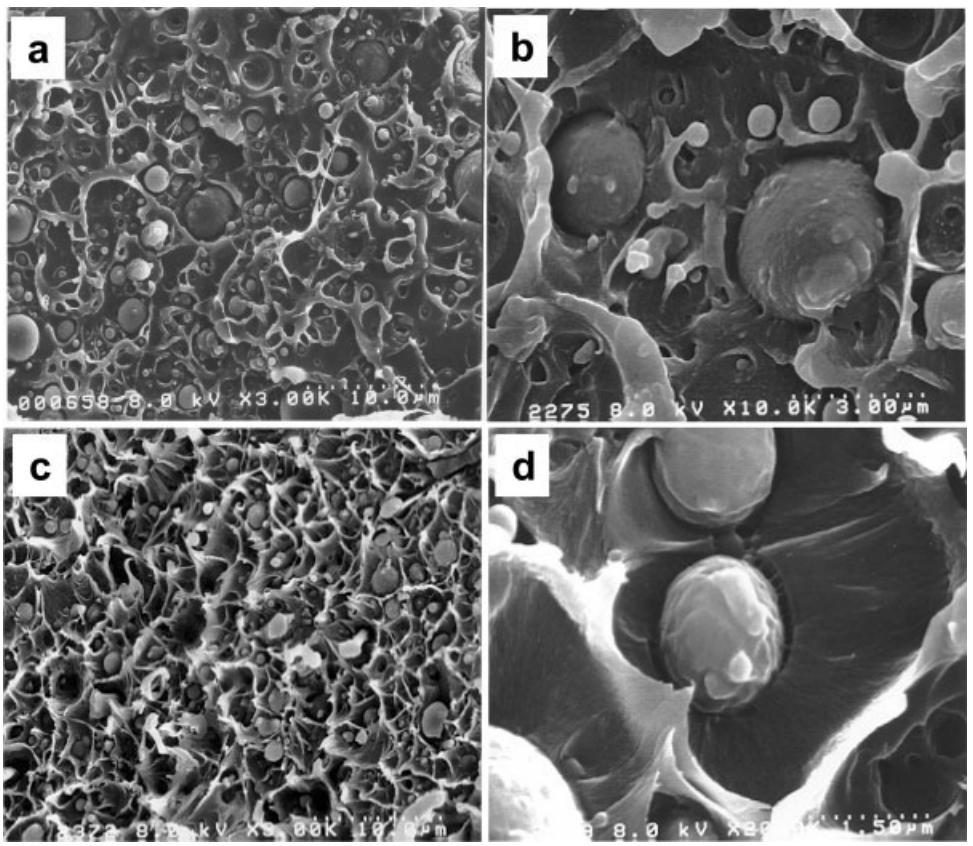

Figure 9 SEM of the impact-fractured surfaces of SEBS-MA compatibilized sPS/PA-6 blends: (a) SEBS-MA 2 wt %, (b) higher magnification of (a), (c) SEBS-MA 5 wt %, and (d) higher magnification of (c).

melting temperatures (T_{m1}, T_{m2}, T_{m3}) decrease with the increase of compatibilizer concentration and a broadening of the melting temperature range is distinct. The melting temperature (T_m) depends on the thickness and perfect (defect) of the crystalline lamella. The broadening of the melting temperature range limits the growth of crystalline domains as revealed by the reduced T_m. The influence of compatibilizer concentration on the crystallization temperature (T_c) and percentage crystallinity (χ_c) of sPS is plotted in Figure 11. The crystallization temperature (T_c) and percentage crystallinity (χ_c) of sPS are drastically reduced at 5% compatibilizer loading. It is likely that the polystyrene tethered chain of SEBS-MA retards the crystallization rate of sPS and hence results in reduced T_c and χ_c of sPS. These changes, in turn points out that the crystallization of sPS is inhibited by the presence of SEBS-MA, by generating numerous small and imperfect crystallites. As we have already discussed, the decrease in T_c and χ_c of sPS occurring between 2 and 5 wt % SEBS-MA concentration also contributes towards the change in fracture mode from brittle to tough in the impact failure of the blends. Hence we can conclude that SEBS-MA as compatibilizer affects the crystal lamellar perfection in the blend.

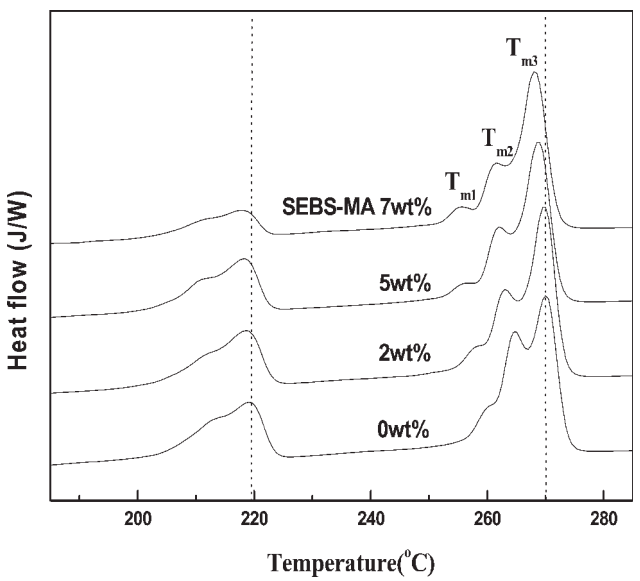

Figure 10 DSC second heating curves of simple and SEBS-MA compatibilized sPS/PA-6 (80/20) blends.

Thin film study

The WAXD off-specular spectra were obtained at a grazing angle of 0.15°, for the sPS with and without

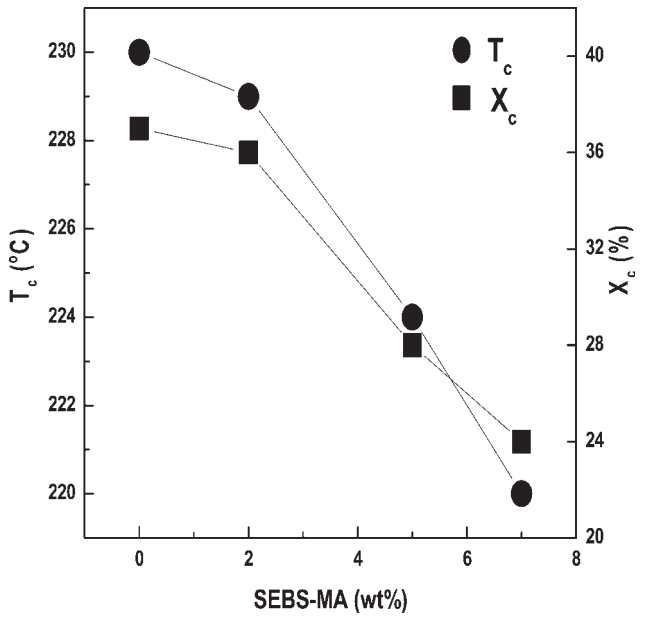

Figure 11 Crystallization temperature and percentage crystallinity of the sPS in sPS/PA-6 (80/20) blends as a function of SEBS-MA content.

SEBS tethered chain. Thin films of ~ 100 nm were used for this study.

As mentioned previously, aPS portion in SEBS-MA is highly miscible with PS, thus it can form an interdiffusion layer with PS above its melting temperature. Once the interfacial layer is formed, the effect from the interdiffusion would be so significant within the thin films of ~ 100 nm thickness that the change in sPS crystalline structure is expected to be well observed.

Figure 12 shows the WAXD results for thin films of sPS, and significant change in the first peak ($2\theta \sim 6.7$, characteristic peak of α-form, obtained by thermal crystallization) was observed as expected; In the case of sPS films crystallized on bare silicon wafers with a film thickness of 100 nm, the half width of the first peak is quite small whereas, for sPS films crystallized on silicon wafers containing tethered SEBS-MA chains, the half width of the first peak appears to be relatively larger.

Half-width of a peak in WAXD spectra is generally indicative of the relative perfection of the corresponding crystalline structure. Thus it can be deduced from Figure 12 that crystalline structure of sPS become more imperfect when sPS is crystallized upon the surface composed of SEBS-MA. This implies that the aPS portion of the tethered chains around the surface hinder perfect chain folding of sPS chains to form crystals, which results in lamellar crystal imperfection. These WAXD result supports our suggestion (from DSC result) on the hindered or retarded crystallization behavior of sPS/PA-6 blends compatibilized with SEBS-MA by envisaging the molecular structure of the interfacial layers.

Therefore, it can be suggested that the crystalline perfection of lamellae near the interface plays an important role in the toughening of sPS blends.

The criterion of toughening to sPS/PA-6 blends

The investigation on the effect of compatibilizer loading on the toughening revealed that for sPS/PA-6 80/20 and 70/30 blends, there is a strong jump of impact strength between 2 and 5 wt % loading of SEBS-MA and for sPS/PA-6 90/10 blends, the abrupt improvement in impact strength occurs at 7 wt % compatibilizer loading (Fig. 8). It can also be noted that sPS/PA-6 80/20 possess much higher impact energy than sPS/PA-6 90/10 blends. This behavior manifests that the improvement in impact strength on compatibilization cannot be ascribed entirely to the better interfacial adhesion and the morphology of the system. These results can be better explained by toughening criterion such as ID and crystalline microstructure.

Interparticle distance

The findings of Wu showed that the toughening effect did not correlate directly with either the rubber particle size or with its volume fraction, but rather with the distance between the particles (ID). He proposed that ID, which is also referred to as the matrix ligament thickness, is the key parameter determining whether a blend is brittle or tough and the critical interparticle distance (ID_c) is the property of the matrix alone. When the interparticle distance is larger than a critical value (ID_c), the fracture mode

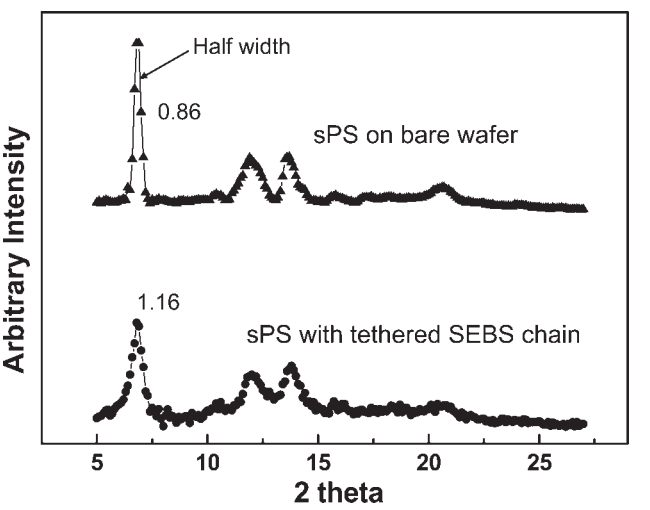

Figure 12 WAXD crystalline peaks for sPS thin film in the presence and absence of SEBS tethered chain.

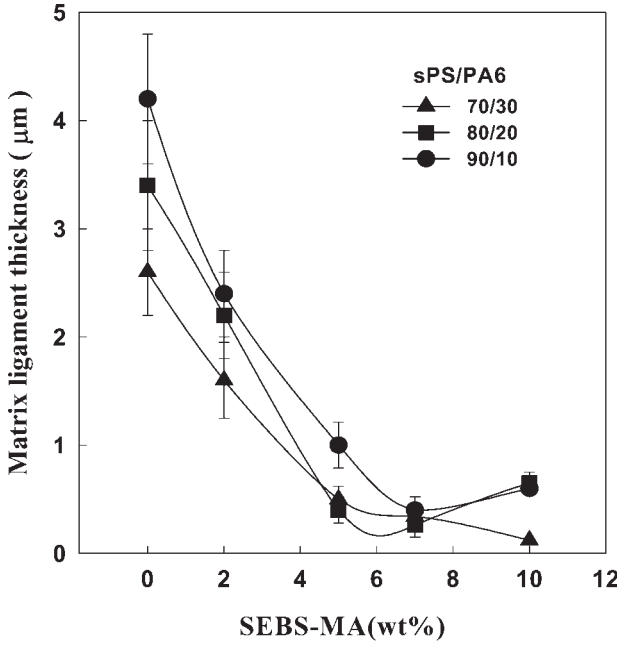

Figure 13 Matrix ligament thickness (ID) as a function of sPS/PA-6 weight ratio and SEBS-MA content.

will be brittle and if ID is less than ID_c, the fracture mode will be tough.

To study the effect of ID on the brittle to tough transition, we calculated the ID values using the following equation[14,15]

$$\mathrm{ID} = d_0\left[\beta\left(\frac{\pi}{6\phi_r}\right)^{1/3}\right]\exp\left(\ln\sigma^2\right)$$

where, d_0 is the number average domain diameter of the particles, β is a geometric constant, depending on the assumed packing of the particles (1.0 for cubic lattice, 1.09 for body-centered cubic and 1.12 for face-centered cubic packing; β is taken as 1 here), ϕ_r is the volume fraction of the particles and σ is the geometrical standard deviation of the particle size distribution. The parameter d_0 is taken from Figure 3.

In Figure 13 the ID of the blends is plotted as a function of sPS/PA-6 composition and SEBS-MA content. It can be observed that SEBS-MA addition has resulted in a reduction of ID. With the addition of 5 wt % compatibilizer, the ID of the blends decreased drastically. The effect of matrix ligament thickness on impact strength is demonstrated in Figure 14, which shows that for all the blend compositions, the notched impact strength increases considerably with the decrease of ID. Figure 14 demonstrates that the data of izod impact strength, obtained for the sPS/PA-6 blends in a broad range of composition follows a single curve when plotted as a function of ID. Our results agree quite well with the findings by Wu and hence, as proposed by him, the criterion of ID for toughening of semicrystalline polymers can be applied successfully to sPS/PA-6/SEBS-MA blends. The master curve presented in the Figure 14 exhibits the toughness jumps when the average ligament thickness decreases below 0.25 μm, which can be considered as the ID_c for the specific sPS matrix used here. ID_c for the system studied is lower than those reported previously for PA 6,6 (ID_c = 0.3 μm)[14] and high density polyethylene (HDPE) (ID_c = 0.6 μm).[13] This in turn suggests that ID_c is a matrix specific parameter. It can also be noted from Figure 13 that on addition of 5 wt % SEBS-MA to sPS/PA-6 90/10 blends the ID is larger than the ID_c. Since the ID for 90/10 blends reaches the critical value only after the incorporation of 7 wt % compatibilizer, the toughness jump for this particular composition occurs at 7 wt % SEBS-MA loading whereas the same takes place at 5 wt % compatibilizer loading in the case of sPS/PA-6 80/20 and 70/30 blends (Fig. 8).

Crystalline microstructure near the particle/matrix interface

Muratoglu et al.[16,17] proposed a morphological explanation for Wu's findings based on the critical ligament dimension. They reported that, in the blends of polyamide 66 and ethylene/propylene anhydride functionalized rubber, the interparticle regions of closely spaced particles exhibit a different morphology, in which the lamellae are organized parallel to

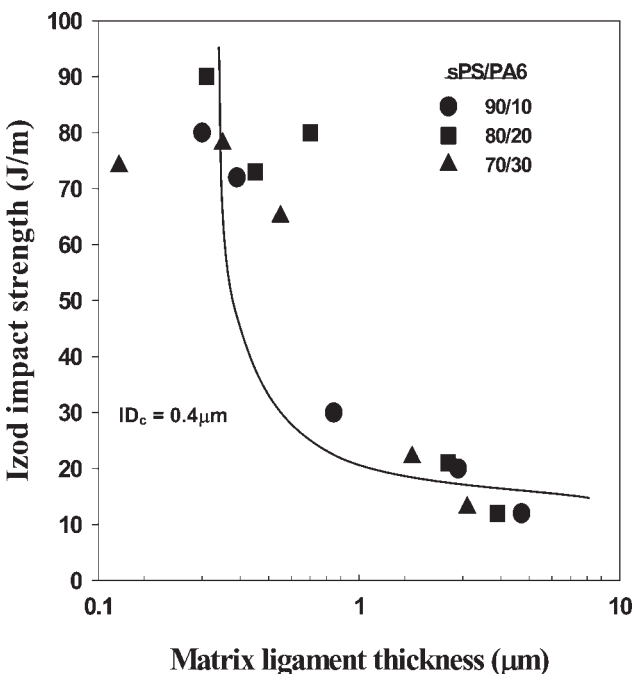

Figure 14 The ''master plot'' of Izod impact strength versus matrix ligament thickness.

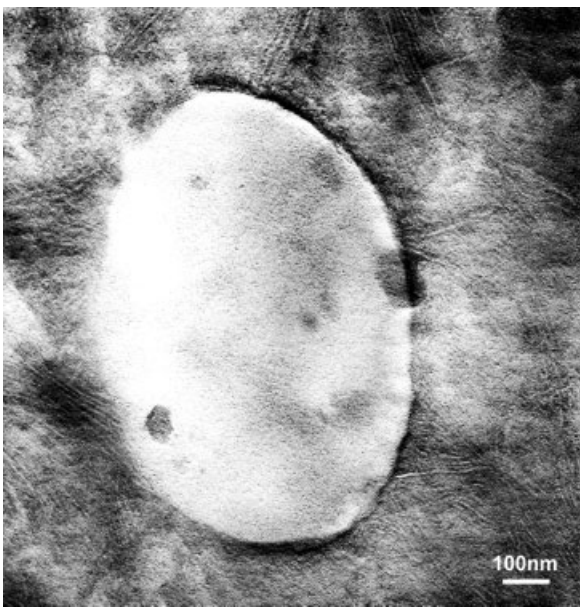

Figure 15 TEM of sPS/PA-6 (80/20) blend compatibilized with 2 wt % SEBS-MA.

each other and perpendicular to the rubber/matrix interface. They correlated their observations with the findings of Wu regarding the ID_c. Accordingly, when the effective ID is below the critical value (0.3 μm for the system studied), the entire sample would behave tough via the percolation of the favorably oriented interparticle regions throughout the specimen. On the other hand, percolation of readily deformable material could not be achieved in brittle samples where the particles are sparsely distributed with much of the background matrix being oriented randomly, having a high deformation resistance. In the case of rubber modified HDPE blends, Bartczak et al.[13] have reported that the high levels of toughness obtained, results from the specific oriented crystallization found in the matrix layers of certain thickness around each rubber inclusion. They found that when the mean ligament thickness is below 0.6 μm (ID_c in this case), the oriented anisotropic material with reduced plastic resistance percolate through the structure, which in turn results in improved toughness. Recent studies on toughened polyamide systems by Leibler and coworkers suggested that toughness of reinforced semicrystalline polymers depend on the crystalline orientation on intermediate scales.[45]

Figure 15 shows a local orientation of sPS lamellae near the interface in sPS/PA-6/SEBS-MA blends (2 wt % SEBS-MA). In TEM micrographs, the dark lines represent the amorphous regions and the white lines represent the lamellae. It can be observed from the Figure that the orientation of the all the lamellae grown near particle/matrix interface is not perpendicular to the interface. This result deviates from the observations of Muratoglu et al. who have conducted the TEM studies on annealed spin-coated PA-6 blend films. In the case of real systems toughened by particle addition, the amount of perpendicular oriented lamellae near particle/matrix interface having curvature will be less than that in a flat surface. This is due to the fact that the growth of lamellae generated at curved surface can be hindered easily by the impingement of nearby lamellae. Hence, the orientation of all lamellae grown near the particle/matrix interface is not perpendicular to the dispersed particles/interface. Nevertheless, when the ID is below 0.25 μm, the fraction of oriented lamellae stacks parallel to each other is dominant and the oriented matrix shells around the inclusions come into contact. As a result, the ID between the inclusions will be partly filled with well-oriented crystalline material of reduced plastic resistance, which then percolates through the whole blend as can be seen from the TEM micrograph of sPS/PA-6 (80/20) blend compatibilized with 7 wt % SEBS-MA (Fig. 16).

The DSC studies showed that addition of 5 and 7 wt % SEBS-MA resulted in the decrease of melting (T_m) and crystallization (T_c) temperatures and crystallinity and also in broadening of the melting temperature range of sPS. A dramatic reduction in crystallinity and T_c occurred between 2 and 5 wt % loading of the compatibilizer and this has been attributed to the existence of more imperfect crystalline region near particle/matrix interface. It is well established that sPS and PA-6 are immiscible and does not entangle in each other due to significant differences in their polarity and solubility parameters.

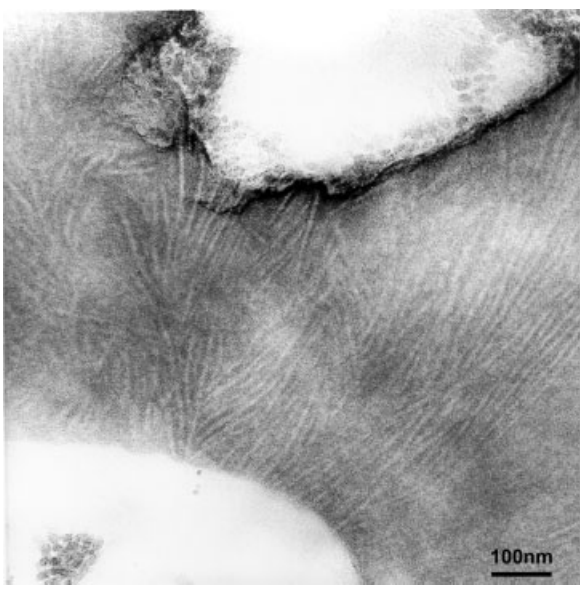

Figure 16 TEM of sPS/PA-6 (80/20) blend compatibilized with 7 wt % SEBS-MA.

The introduction of SEBS-MA at the interface mediates an attractive interaction between the immiscible sPS and PA-6. During melt mixing, sPS is miscible with aPS by means of diffusion process. The quality of the SEBS/sPS interface depends on the triblock end segments (PS) forming mechanical entanglements with the matrix (sPS) material. The addition of SEBS-MA causes an increase in interfacial thickness by the pronounced penetration of the triblock end segments (aPS) into the sPS phase. The WAXD studies on the model system indicate that the interaction between aPS and sPS segments can hinder the perfect chain folding of sPS (Fig. 12). It has already been noted that the SEBS-MA addition resulted in a decrease of particle size of the dispersed phase. This can lead to an increased volume fraction of the interface near the particle/matrix. Therefore it can be stated that the decrease of T_m, T_c, and χ_c as well as the broadening of melting temperature range of sPS in the compatibilized blends can be attributed to the penetration of the triblock end segments of the compatibilizer into sPS phase. Consequently, these changes imply that the crystallization of sPS is inhibited by the addition of SEBS-MA, leading to the formation of many (numerous) small and imperfect crystallites near the particle/matrix interface. Hence, we suggest that the resulting lamellae morphology might have originated from the different crystal orientation and imperfect crystals of the matrix sPS at the interface with the change in ID.

CONCLUSION

Impact strength of sPS can be improved by the addition of PA-6 employing SEBS-MA as the compatibilizer without any substantial reduction in modulus. Morphology studies revealed that a significant reduction in the domain size as well as a uniform distribution of the dispersed phase could be obtained at a compatibilizer concentration beyond 2 wt %, indicating a strong interfacial adhesion between the components. Toughness jump in sPS/PA-6 80/20 and 70/30 blends occurred between 2 and 5 wt % of compatibilizer incorporation and for 90/10 blends it was between 5 and 7 wt % SEB-MA addition. This is associated with the change in fracture mode of the blends from brittle to tough, leading to the shear yielding fracture of the matrix.

By applying of the criterion of ID for toughening in sPS/PA-6/SEBS-MA blends, we obtained a value 0.25 μm as the ID_c, below which all the blends were found to be tough. Investigations on the effect of crystalline microstructure in the blends revealed that when the ID is below 0.25 μm, the fraction of oriented lamellae stacks parallel to each other is dominant and the oriented matrix shells around the inclusions come into contact. As a result, the matrix ligaments between the inclusions will be partly filled with well-oriented crystalline material of reduced plastic resistance, which then percolates throughout the whole blend. This in turn also contributed to the improvement in toughness of the blends. Studies on crystalline microstructure using DSC and X-ray diffraction pointed out that the crystallization of sPS is inhibited by the presence of SEBS-MA by creating numerous small and imperfect crystallites, which manifested a decrease in T_m, T_c, and χ_c of the compatibilzed blends. This inhibition is caused by the entanglement of the triblock end segments (aPS) of the compatibilizer with the sPS phase. From these results, it could be concluded that the improvement in toughness of the sPS/PA-6/SEBS-MA blends could be attributed to the ID, crystal orientation and imperfect crystals of the sPS matrix ultimately leading to the reduction of yield stress with increasing concentration of the SEBS-MA, which is accompanied by the change in fracture mode from brittle to tough.

The authors thank the Pohang Accelerator Laboratory for providing the 3C2 beam line used in this study.

References

1. Ishihara, N.; Seimiya, T.; Kuramoto, M.; Uoi, M. Macromolecules 1986, 199, 2464.
2. Pellecehia, C.; Longo, P.; Grassi, A.; Ammendola, P.; Zambelli, A. Makromol Chem Rapid Commun 1987, 8, 277.
3. Zambelli, A.; Longo, P.; Pellecehia, C.; Grassi, A.; Macromolecules 1987, 20, 2035.
4. Ishihara, N.; Kuramoto, M.; Uoi, M. Macromolecules 1988, 21, 3356.
5. Reynolds, N. M.; Hsu, S. L. Macromolecules 1990, 23, 3463.
6. Sun, Z.; Morgan, R. J.; Lewis, D. N. Polymer 1992, 33, 725.
7. Jones, M. A.; Carriere, C. J.; Dinnen, M. T.; Balwinski, K. M. J Appl Polym Sci 1997, 64, 673.
8. Zhang, X. Q.; Son, Y. J Appl Polym Sci 2003, 89, 2502.
9. Li, H. M.; Shen, Z.; Zhu, F.; Lin, S. Eur Polym Mater 2002, 38, 1255.
10. Xu, S.; Chen, B.; Liu, Y.; Chen, H.; Huang, B. Polymer 1999, 40, 3399.
11. Hong, B. K.; Jo, W. H. Polymer 2000, 41, 2069.
12. Ramsteiner, F.; McKee, G. E.; Heckmann, W.; Oepen, S.; Geprags, M. Polymer 2000, 41, 6635.
13. Bartczak, Z.; Argon, A. S.; Cohen, R. E.; Weinberg, M. Polymer 1999, 40, 2331.
14. Wu, S. Polymer 1985, 269, 1855.
15. Wu, S. J Appl Polym Sci 1988, 35, 549.
16. Muratoglu, O. K.; Argon, A. S.; Cohen, R. E.; Weinberg, M. Polymer 1995, 36, 921.
17. Muratoglu, O. K.; Argon, A. S.; Cohen, R. E.; Weinberg, M. Polymer 1995, 36, 4771.
18. Majumdar, B.; Keskkula, H.; Paul, D. R. Polymer 1994, 35, 1399.
19. Jiang, W.; Yu, D.; Jiang, B. Polymer 2004, 45, 6427.
20. Loyens, W.; Groeninckx, G. Polymer 2003, 44, 123.
21. Cho, K.; Yang, J. H.; Yoon, S.; Hwang, M.; Sobha, N. V. J Appl Polym Sci 2005, 95, 748.
22. Cho, K.; Yang, J. H.; Kang, B. I.; Park, C. E. J Appl Polym Sci 2003, 89, 3115.
23. Cho, K.; Yang, J. H.; Park, C. E. Polymer 1998, 39, 3073.

24. Cho, K.; Yang, J. H.; Park, C. E. Polymer 1997, 38, 5161.
25. Borggreve, R. J. M.; Gaymans, R. J.; Schuijer, J.; Housz, J. I. Polymer 1987, 28, 1489.
26. Woo, E. M.; Wu, F. S. Macromol Chem Phys 1998, 199, 2041.
27. Sue, H. J.; Yee, A. F. J Mater Sci 1991, 26, 3449.
28. Sue, H. J.; Pearson, R. A.; Yee, A. F. Polym Eng Sci 1991, 31, 793.
29. Wei, G. X.; Sue, H. J.; Chu, J. J Mater Sci 2000, 35, 555.
30. Nair, S. V.; Wong, S. C.; Gottler, L. A. J Mater Sci 1997, 32, 5335.
31. Dutt, G.; Kit, K. M. J Appl Polym Sci 2003, 879, 1984.
32. Han, J. T.; Cho, K. J Mater Sci 2006, 41, 4239.
33. Han, J. T.; Cho, K. Macromol Mater Eng 2005, 290, 1184.
34. Sundararaj, U.; Macosko, C. W. Macromolecules 1995, 28, 2647.
35. Teyssie, P.; Fyat, R.; Jerome, R. Macromol Chem 1986, 187, 837.
36. Thomas, S.; Groeninckx, G. Polymer 1999, 40, 5799.
37. Jeon, H. K.; Feist, B. J.; Koh, S. B.; Chang, K.; Macosko, C. W.; Dion, R. P. Polymer 2004, 45, 197.
38. Ide, F.; Hasegawa, A. J Appl Polym Sci 1974, 18, 963.
39. Wang, C.; Liao, W. P.; Cheng, Y. W.; Lin, T. L. Polymer 2004, 45, 961.
40. de Candia, F.; Ruvolvo, F. A.; Vittoria, V. Colloid Polym Sci 1991, 269, 650.
41. Li, H.; Li, Z. J Appl Polym Sci 1998, 67, 61.
42. Parker, D. S.; Sue, H. J.; Huang, J.; Yee, A. Polymer 1990, 31, 2267.
43. Heino, M.; Hietaoja, P.; Seppala, J.; Harima, T.; Friedrich, K. J Appl Polym Sci 1997, 66, 2209.
44. Greco, R.; Mancarella, C.; Matruscelli, E.; Ragosta, G.; Yin, J. Polymer 1987, 28, 1929.
45. Corte, L.; Beaumeb, F.; Leibler, L. Polymer 2005, 46, 2748.
46. Kolarik, J.; Fambri, L.; Slouf, M.; Konecny, D. J Appl Polym Sci 2005, 96, 673.